

# Demosaicing: Image Reconstruction from Color CCD Samples

Ron Kimmel

**Abstract**— A simplified color image formation model is used to construct an algorithm for image reconstruction from CCD sensors samples. The proposed method involves two successive steps. The first is motivated by Cok's template matching technique, while the second step uses steerable inverse diffusion in color. Classical linear signal processing techniques tend to oversmooth the image and result in noticeable color artifacts along edges and sharp features. The question is how should the different color channels support each other to form the best possible reconstruction. Our answer is to let the edges support the color information, and the color channels support the edges, and thereby achieve better perceptual results than those that are bounded by the sampling theoretical limit.

**Index Terms**— Color enhancement, image reconstruction, multichannel nonlinear image processing, steerable inverse diffusion.

## I. INTRODUCTION

IN RECENT years, digital cameras for still images and movies became popular. There are many obvious advantages to digital images comparing to classical film based cameras, yet there are limitations as well. For example, the spatial resolution is limited due to the physical structure of the sensors. "Superresolution" beyond the sensors resolution can be achieved by considering a sequence of images.

In this work, we deal with the reconstruction of a single color digital image from its color CCD sensors' information. We limit our discussion to Bayer color filter array (CFA) pattern as presented in Fig. 1. We will start with a simple color image formation model and explore the relation between the different color channels such that the channels support the edges, and the edges support the colors. This relation with a simple color image formation model enables a reconstruction beyond the linear optimal signal processing approach that is limited by the Nyquist sampling rate.

We follow Cok's [1] exposition for constructing the first step of the algorithm: the reconstruction stage. The green component is reconstructed first with the help of the red and

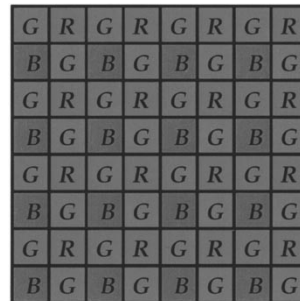


Fig. 1. Bayer CFA (color filter array) pattern (U.S. Patent 3 971 065, 1976).

blue gradients. Then the red and blue are reconstructed using the green values, edge approximations, and a simple color ratio rule: Within a given "object" the ratio *red/green* is locally constant (the same is true for *blue/green*). This rule falls apart across edges where the color gradients are high, which are the interesting and problematic locations from our reconstruction point of view.

Next, the green, red, and blue pixels are adjusted to fit the color cross ratio equivalence. The interpolation and the adjustment are weighted by a function of the directional derivatives to reduce the influence of ratios across edges. This is the main difference from Cok's [1] method, who try to match templates that predict the local structure of the image for a bilinear interpolation.

The second step, the enhancement stage, involves an anisotropic inverse diffusion flow in color space, which is an extension of Gabor's geometric filter [6], and is based on the geometric framework for color introduced in [8] and [11]. It is also related to Weickert's texture enhancement method [12], and to the recent results of Sapiro and Ringach [10], and Cottet and El Ayyadi [2]. The idea is to consider the color image as a two-dimensional (2-D) surface in five-dimensional (5-D)  $(x, y, R, G, B)$  space, extract its induced metric and smooth the metric in order to sense the structure of the image surface beyond the local noise. Then diffuse the different channels along the edges and simultaneously enhance the image by applying an "inverse heat" operator across the edges.

The structure of this paper is as follows. Section II introduces a simple model for color images. Next, Section III uses this model for the reconstruction of a one-dimensional (1-D) image. Section IV presents the first step of the algorithm, the reconstruction stage, that involves weighted interpolation subject to constant cross ratio of the spectral channels. Section V presents the second step of the algorithm. It is a

Manuscript received September 25, 1997; revised October 21, 1998. This work was supported in part by the Israeli Ministry of Science, by the OER Applied Mathematics Subprogram DE-AC03-76SF00098, and by the Office of Naval Research under Grant N00014-96-1-0381. Part of this work was conducted while the author was affiliated with Lawrence Berkeley Laboratories and the Mathematics Department, University of California, Berkeley. The associate editor coordinating the review of this manuscript and approving it for publication was Prof. Stephen E. Reichenbach.

The author is with the Computer Science Department, Technion, Haifa 32000, Israel (e-mail: ron@cs.technion.ac.il).

Publisher Item Identifier S 1057-7149(99)06817-7.

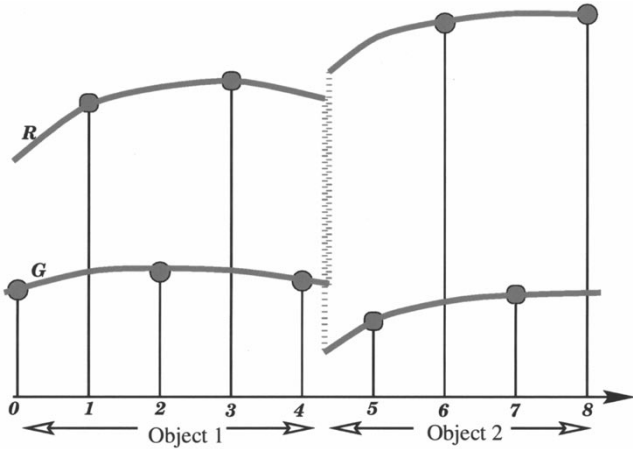


Fig. 2. Red and green components of a 1-D image. This figure can be seen in color at [www.cs.technion.ac.il/~ron/demosaic.html](http://www.cs.technion.ac.il/~ron/demosaic.html).

nonlinear enhancement filter based on steerable anisotropic inverse diffusion flow in color space. Section V concludes with experimental results on a set of benchmark images.<sup>1</sup>

## II. SIMPLE COLOR IMAGE FORMATION MODEL

A simplified model for color images is a result of viewing Lambertian nonflat surface patches. Such a scene is a generalization of what is known as a “Mondriaan world.” According to the model, each channel may be considered as the projection of the real three-dimensional (3-D) world surface normal  $\hat{\mathbf{N}}(\mathbf{x})$  onto the light source direction  $\vec{l}$ , multiplied by the albedo  $\rho(x, y)$ . The albedo captures the characteristics of the 3-D object’s material, and is different for each of the spectral channels. That is, the three color channels may be written as

$$\begin{aligned} I^R(\mathbf{x}) &= \rho_R(\mathbf{x}) \langle \hat{\mathbf{N}}(\mathbf{x}), \vec{l} \rangle \\ I^G(\mathbf{x}) &= \rho_G(\mathbf{x}) \langle \hat{\mathbf{N}}(\mathbf{x}), \vec{l} \rangle \\ I^B(\mathbf{x}) &= \rho_B(\mathbf{x}) \langle \hat{\mathbf{N}}(\mathbf{x}), \vec{l} \rangle. \end{aligned} \quad (1)$$

This means that the different colors capture the change in material via  $\rho_i$  (where  $i$  stands for  $R, G, B$ ) that multiplies the normalized shading image  $\tilde{I}(\mathbf{x}) = \langle \hat{\mathbf{N}}(\mathbf{x}), \vec{l} \rangle$ . The Mondriaan color image formation model [4] was used for color based segmentation [7] and shading extraction from color images [5]. Let us follow the above generalization of this model and assume that the material, and therefore the albedo, are the same within a given object in the image, e.g.,  $\rho_i(\mathbf{x}) = c_i$ , where  $c_i$  is a given constant. Thus, within the interior of a given object the following constant ratio holds:

$$\frac{I^i(\mathbf{x})}{I^j(\mathbf{x})} = \frac{\rho_i(\mathbf{x}) \tilde{I}(\mathbf{x})}{\rho_j(\mathbf{x}) \tilde{I}(\mathbf{x})} = \frac{\rho_i(\mathbf{x})}{\rho_j(\mathbf{x})} = \frac{c_i}{c_j} = \text{constant}. \quad (2)$$

That is, the color ratio within a given object is constant. We note, that this is an oversimplified assumption for general analysis of color images. However, its local nature makes it valid and useful for our technological purpose.

<sup>1</sup>Some of the techniques we present were developed as a result of discussions with Prof. J. A. Sethian, University of California—Berkeley, and Dr. Y. Hel-Or, IDC Israel.

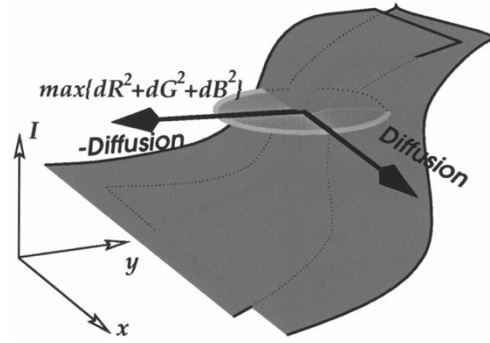


Fig. 3. Red and green components painted as surfaces in  $x, y, I$  with the inverse diffusion (across the edge) and diffusion (along the edge) directions.

## III. THE 1-D CASE

Let us start with a simple 1-D example with two colors; see Fig. 2. Our assumption is that the colors are smooth within a given object and go through a sudden jump at the boundaries. Define the central difference approximation to be  $D_x I_i \equiv (I_{i+1} - I_{i-1})/\Delta x$ , where  $I_i \equiv I(i\Delta x)$  is the value of the function  $I(x)$  at the point  $x = i\Delta x$ , and  $\Delta x$  is the spatial discretization interval.

Given the samples (odd points for the red and even points for the green) we use the gradient to construct an edge indicator for the interpolation. Let the edge indicator be  $e_i^g = f(D_x G_i)$ , where  $f(\circ)$  is a decreasing function, e.g.,  $e_i^g = (1 + (D_x G_i)^2)^{-1/2}$ , and, respectively,  $e_i^r$ . One simple reconstruction procedure is as follows.

- *Init:* Interpolate for the green at the missing points

$$G_i = \frac{e_{i-1}^r G_{i-1} + e_{i+1}^r G_{i+1}}{e_{i-1}^r + e_{i+1}^r}.$$

- *Repeat for three times:*
- Interpolate the red values via the ratio rule weighted by the edge indicator

$$R_i = G_i \frac{e_{i-1}^g \frac{R_{i-1}}{G_{i-1}} + e_{i+1}^g \frac{R_{i+1}}{G_{i+1}}}{e_{i-1}^g + e_{i+1}^g}.$$

- Correct the green values to fit the ratio rule

$$G_i = R_i \frac{e_{i-1}^r \frac{G_{i-1}}{R_{i-1}} + e_{i+1}^r \frac{G_{i+1}}{R_{i+1}}}{e_{i-1}^r + e_{i+1}^r}.$$

- *End of loop.*

Note that this is a numerically consistent procedure for the proposed color image formation model. It means that as the sampling grid is refined, the result converges to the continuous solution.

Here again we recognize the importance of segmentation in computer vision. An accurate segmentation procedure, that gives the exact locations of the objects boundaries, would have allowed an image reconstruction far beyond the sampling limit (under the assumption that within a given object there are no high spatial frequencies).

## IV. FIRST STEP: RECONSTRUCTION

For real 2-D images with three color channels the reconstruction is less trivial. Edges now become curves rather



Fig. 4. Top left: original statue image. Top right: result of a bilinear interpolation for the missing points for each channel. Bottom left: result of the first reconstruction by weighted interpolation step. Bottom right: second step enhancement result. This figure can be seen in color at [www.cs.technion.ac.il/~ron/demosaic.html](http://www.cs.technion.ac.il/~ron/demosaic.html).

than points, and in many cases one needs to interpolate missing points along the edges. We would still like to avoid interpolating across edges.

Based on the simplified color image formation model, the three channels go through a sudden jump across the edges. Thus, the gradient magnitude can be used as an edge indicator, and its direction can approximate the edge direction [it is easy

to verify that the gradient  $\nabla G$  is normal to the level set curves of  $G(\mathbf{x})$ , i.e.,  $G(\mathbf{x}) = \text{const.}$ ]

The directional derivatives are approximated at each point based on its eight nearest neighbors on the grid. Define the finite difference approximation for the directional derivatives, central  $D$ , forward  $D^+$ , and backward  $D^-$ , as in (3), shown at the bottom of p. 1225. At the green points

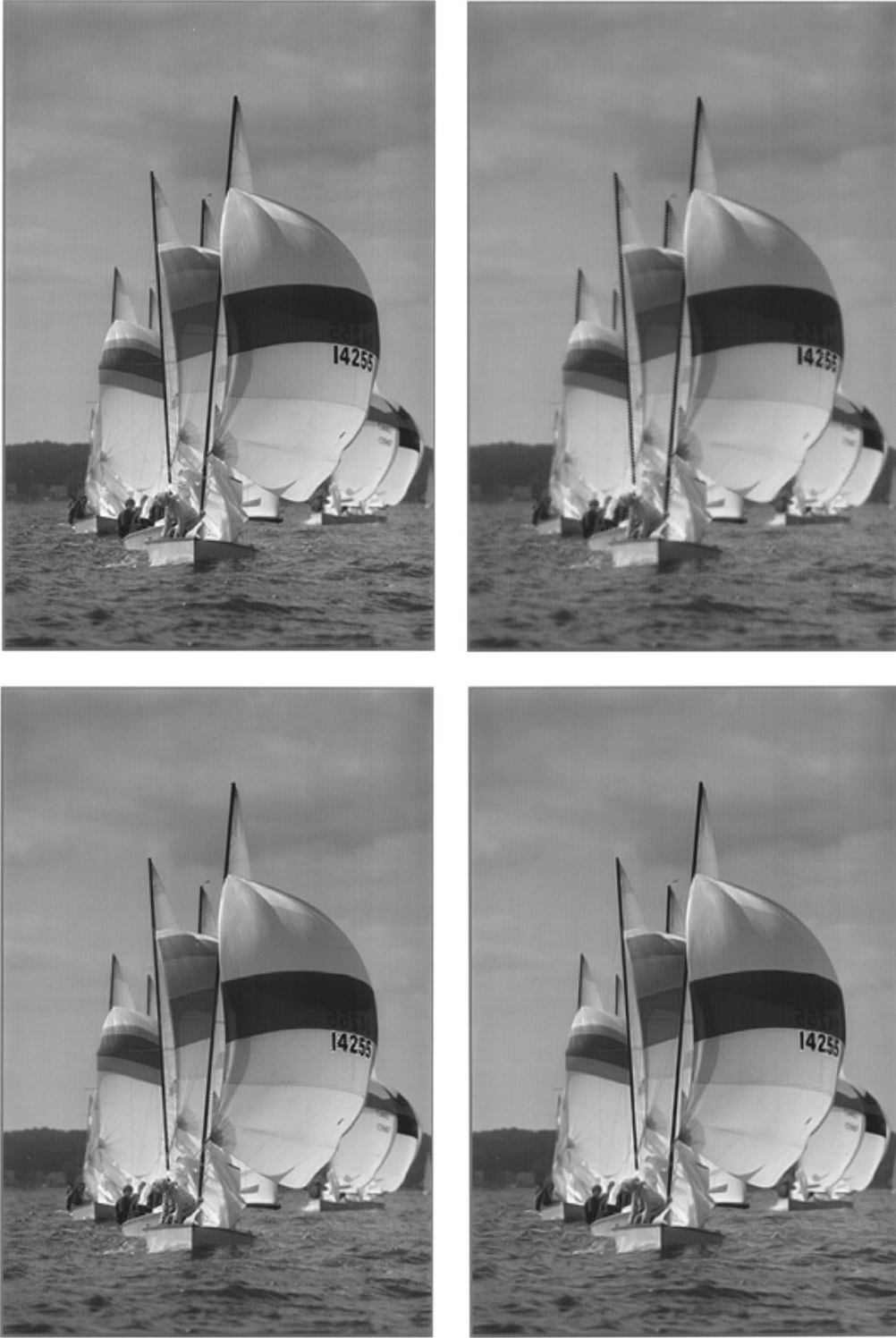


Fig. 5. Top left: original sailboat image. Top right: result of a bilinear interpolation for the missing points for each channel. Bottom left: result of the first reconstruction by weighted interpolation step. Bottom right: second step enhancement result. This figure can be seen in color at [www.cs.technion.ac.il/~ron/demosaic.html](http://www.cs.technion.ac.il/~ron/demosaic.html).

use  $\max\{|D_{x'}^+ G_{i,j}|, |D_{x'}^- G_{i,j}|\}$  for the magnitude of the directional derivative along the  $x'$  direction (and similarly for  $y'$ ). For the rest of the points and the  $x$  and  $y$  directions use central differences. We thereby construct an approximation for the directional derivatives at each and every point. Denote these approximations as  $Dx_{ij}$ ,  $Dy_{ij}$ ,  $Dx'_{ij}$ , and  $Dy'_{ij}$ , respectively.

Next, we generalize an edge indicator function. When a point at location  $((i+1)\Delta x, j\Delta y)$  is taking part in the interpolation at the  $(i\Delta x, j\Delta y)$  location, we use the following weight as an edge indicator:  $c_{ij}^{x+1,j} = (1 + Dx_{ij}^2 + Dx_{i+1,j}^2)^{-1/2}$ .

Based on the edge indicators as weights for the interpolation we follow similar steps as for the 1-D case to reconstruct the 2-D image.



Fig. 6. Top left: original window image. Top right: result of a bilinear interpolation for the missing points for each channel. Bottom left: result of the first reconstruction by weighted interpolation step. Bottom right: second step enhancement result. This figure can be seen in color at [www.cs.technion.ac.il/~ron/demosaic.html](http://www.cs.technion.ac.il/~ron/demosaic.html).

$$\left\{ \begin{array}{ll}
 D_x G_{i,j} = \frac{G_{i+1,j} - G_{i-1,j}}{2\Delta x} & \begin{array}{c} \circ - \circ - \circ \\ | \quad | \quad | \\ \ominus \quad \oplus \quad \ominus \\ | \quad | \quad | \\ \circ - \circ - \circ \end{array} & D_y G_{i,j} = \frac{G_{i,j+1} - G_{i,j-1}}{2\Delta y} & \begin{array}{c} \circ - \oplus - \circ \\ | \quad | \quad | \\ \circ - \oplus - \circ \\ | \quad | \quad | \\ \circ - \ominus - \circ \end{array} \\
 D_{x'} G_{i,j} = \frac{G_{i+1,j+1} - G_{i-1,j-1}}{2\sqrt{\Delta x^2 + \Delta y^2}} & \begin{array}{c} \circ - \circ - \oplus \\ | \quad | \quad | \\ \ominus - \oplus - \ominus \\ | \quad | \quad | \\ \circ - \circ - \circ \end{array} & D_{y'} G_{i,j} = \frac{G_{i-1,j+1} - G_{i+1,j-1}}{2\sqrt{\Delta x^2 + \Delta y^2}} & \begin{array}{c} \oplus - \circ - \circ \\ | \quad | \quad | \\ \ominus - \oplus - \ominus \\ | \quad | \quad | \\ \circ - \circ - \circ \end{array} \\
 D_{x'}^+ G_{i,j} = \frac{G_{i+1,j+1} - G_{i,j}}{\sqrt{\Delta x^2 + \Delta y^2}} & \begin{array}{c} \circ - \circ - \oplus \\ | \quad | \quad | \\ \circ - \oplus - \circ \\ | \quad | \quad | \\ \circ - \circ - \circ \end{array} & D_{x'}^- G_{i,j} = \frac{G_{i+1,j+1} - G_{i,j}}{\sqrt{\Delta x^2 + \Delta y^2}} & \begin{array}{c} \circ - \circ - \circ \\ | \quad | \quad | \\ \circ - \oplus - \circ \\ | \quad | \quad | \\ \circ - \circ - \circ \end{array} \\
 D_{y'}^+ G_{i,j} = \frac{G_{i-1,j+1} - G_{i,j}}{\sqrt{\Delta x^2 + \Delta y^2}} & \begin{array}{c} \oplus - \circ - \circ \\ | \quad | \quad | \\ \circ - \oplus - \circ \\ | \quad | \quad | \\ \circ - \circ - \circ \end{array} & D_{y'}^- G_{i,j} = \frac{G_{i,j} - G_{i+1,j-1}}{\sqrt{\Delta x^2 + \Delta y^2}} & \begin{array}{c} \circ - \circ - \circ \\ | \quad | \quad | \\ \circ - \oplus - \circ \\ | \quad | \quad | \\ \circ - \circ - \circ \end{array}
 \end{array} \right. \quad (3)$$

- *Init:* Interpolate for the green at the missing points as in (3a), shown at the bottom of the page. Interpolate for the blue and red in Steps 1 and 2, shown at the bottom of the page. Interpolate the red with two similar steps.
- *Repeat for three times:*
- Correct the green values to fit the ratio rule

$$G_{ij}^B = B_{ij} \left( e_{ij}^{i+1,j} \frac{G_{i+1,j}}{B_{i+1,j}} + e_{ij}^{i-1,j} \frac{G_{i-1,j}}{B_{i-1,j}} + e_{ij}^{i,j+1} \frac{G_{i,j+1}}{B_{i,j+1}} + e_{ij}^{i,j-1} \frac{G_{i,j-1}}{B_{i,j-1}} + e_{ij}^{i+1,j+1} \frac{G_{i+1,j+1}}{B_{i+1,j+1}} + e_{ij}^{i-1,j-1} \frac{G_{i-1,j-1}}{B_{i-1,j-1}} + e_{ij}^{i-1,j+1} \frac{G_{i-1,j+1}}{B_{i-1,j+1}} + e_{ij}^{i+1,j-1} \frac{G_{i+1,j-1}}{B_{i+1,j-1}} \right) / \left( e_{ij}^{i+1,j} + e_{ij}^{i-1,j} + e_{ij}^{i,j+1} + e_{ij}^{i,j-1} + e_{ij}^{i+1,j+1} + e_{ij}^{i-1,j-1} + e_{ij}^{i+1,j-1} \right) \quad (4)$$

and average between the blue and red interpolation results

$$G_{ij} = \frac{G_{ij}^B + G_{ij}^R}{2}.$$

- Correct the blue and red values via the ratio rule weighted by the edge indicator

$$B_{ij} = G_{ij} \left( e_{ij}^{i+1,j} \frac{B_{i+1,j}}{G_{i+1,j}} + e_{ij}^{i-1,j} \frac{B_{i-1,j}}{G_{i-1,j}} + e_{ij}^{i,j+1} \frac{B_{i,j+1}}{G_{i,j+1}} + e_{ij}^{i,j-1} \frac{B_{i,j-1}}{G_{i,j-1}} + e_{ij}^{i+1,j+1} \frac{B_{i+1,j+1}}{G_{i+1,j+1}} + e_{ij}^{i-1,j-1} \frac{B_{i-1,j-1}}{G_{i-1,j-1}} + e_{ij}^{i-1,j+1} \frac{B_{i-1,j+1}}{G_{i-1,j+1}} + e_{ij}^{i+1,j-1} \frac{B_{i+1,j-1}}{G_{i+1,j-1}} \right) / \left( e_{ij}^{i+1,j} + e_{ij}^{i-1,j} + e_{ij}^{i,j+1} + e_{ij}^{i,j-1} + e_{ij}^{i+1,j+1} + e_{ij}^{i-1,j-1} + e_{ij}^{i+1,j-1} + e_{ij}^{i-1,j+1} + e_{ij}^{i+1,j-1} \right). \quad (5)$$

- *End of loop.*

Up to this point, the original values given as samples were not modified. We have interpolated the missing points weighted by edge indicator functions subject to the constant cross ratio. Next, we apply inverse diffusion in color to the whole image as an enhancement filter.

## V. SECOND STEP: ENHANCEMENT

This section is a brief description of one of the nonlinear filters introduced in [8] that we apply as a second step for enhancing the color image.

In [6], Gabor considered an image enhancement procedure based on an anisotropic flow via the *inverse* second directional derivative in the “edge” direction and the geometric heat equation as a diffusion along the edge, see also [9]. Cottet and Germain [3] used a smoothed version of the image to direct the diffusion. Weickert [12] smoothed the “structure tensor”  $\nabla I \nabla I^T$  and then manipulated its eigenvalues to steer the smoothing direction, while Sapiro and Ringach [10] eliminated one eigenvalue from the structure tensor in color space without smoothing its coefficients.

Motivated by all of these results, a new color enhancement filter was introduced in [8]. The inverse diffusion and diffusion directions are deduced from the smoothed metric coefficients  $g_{\mu\nu}$  of the image surface. The color image is considered as a 2-D surface in the 5-D  $(x, y, R, G, B)$  space, as suggested in [11]. The induced metric coefficients are extracted for the image surface and used as a natural structure tensor for the color case.

The induced metric  $(g_{\mu\nu})$  is a symmetric matrix that captures the geometry of the image surface. Let  $\lambda_1$  and  $\lambda_2$  be the largest and the smallest eigenvalues of  $(g_{\mu\nu})$ , respectively. Since  $(g_{\mu\nu})$  is a symmetric positive matrix its corresponding eigenvectors  $u_1$  and  $u_2$  can be chosen orthonormal. Let  $U \equiv (u_1 | u_2)$ , and  $\Lambda \equiv \begin{pmatrix} \lambda_1 & 0 \\ 0 & \lambda_2 \end{pmatrix}$ , then we readily have the equality

$$(g_{\mu\nu}) = U \Lambda U^T. \quad (6)$$

---


$$G_{ij} = \frac{e_{ij}^{i-1,j} G_{i-1,j} + e_{ij}^{i+1,j} G_{i+1,j} + e_{ij}^{i,j-1} G_{i,j-1} + e_{ij}^{i,j+1} G_{i,j+1}}{e_{ij}^{i-1,j} + e_{ij}^{i+1,j} + e_{ij}^{i,j-1} + e_{ij}^{i,j+1}} \quad (3a)$$


---

*Step 1—Interpolate Missing Blue at Red Locations:*

$$B_{ij} = G_{ij} \frac{e_{ij}^{i+1,j+1} \frac{B_{i+1,j+1}}{G_{i+1,j+1}} + e_{ij}^{i-1,j-1} \frac{B_{i-1,j-1}}{G_{i-1,j-1}} + e_{ij}^{i-1,j+1} \frac{B_{i-1,j+1}}{G_{i-1,j+1}} + e_{ij}^{i+1,j-1} \frac{B_{i+1,j-1}}{G_{i+1,j-1}}}{e_{ij}^{i+1,j+1} + e_{ij}^{i-1,j-1} + e_{ij}^{i-1,j+1} + e_{ij}^{i+1,j-1}}.$$

*Step 2—interpolate at the rest of the missing blue points:*

$$B_{ij} = G_{ij} \frac{e_{ij}^{i+1,j} \frac{B_{i+1,j}}{G_{i+1,j}} + e_{ij}^{i-1,j} \frac{B_{i-1,j}}{G_{i-1,j}} + e_{ij}^{i,j+1} \frac{B_{i,j+1}}{G_{i,j+1}} + e_{ij}^{i,j-1} \frac{B_{i,j-1}}{G_{i,j-1}}}{e_{ij}^{i+1,j} + e_{ij}^{i-1,j} + e_{ij}^{i,j+1} + e_{ij}^{i,j-1}}.$$



Fig. 7. Top left: original lighthouse image. Top right: result of a bilinear interpolation for the missing points for each channel. Bottom left: result of the first reconstruction by weighted interpolation step. Bottom right: second step enhancement result. This figure can be seen in color at [www.cs.technion.ac.il/~ron/Demosaic/](http://www.cs.technion.ac.il/~ron/Demosaic/).

Note also that

$$(g^{\mu\nu}) \equiv (g_{\mu\nu})^{-1} = U\Lambda^{-1}U^T = U \begin{pmatrix} 1/\lambda_1 & 0 \\ 0 & 1/\lambda_2 \end{pmatrix} U^T \quad (7)$$

and that

$$g \equiv \det(g_{\mu\nu}) = \lambda_1\lambda_2. \quad (8)$$

Let us use the image metric as a structure tensor. We extract the structure from the metric  $(g_{\mu\nu})$  and then modify it to be a nonsingular symmetric matrix with one positive and one *negative* eigenvalues. That is, instead of diffusion we introduce an inverse diffusion in the edge direction (across the edge). This is an extension of Gabor's idea [6] of inverting the diffusion along the gradient direction; see Fig. 3.

$$(g_{\mu\nu}) = \begin{pmatrix} 1 + R_x^2 + G_x^2 + B_x^2 & R_x R_y + G_x G_y + B_x B_y \\ R_x R_y + G_x G_y + B_x B_y & 1 + R_y^2 + G_y^2 + B_y^2 \end{pmatrix}. \quad (10)$$

The proposed inverse diffusion enhancement for color images is then given as follows.

- 1) Compute the metric coefficients  $g_{\mu\nu}$ .

$$g_{\mu\nu} = \delta_{\mu\nu} + \sum_{k=\{R, G, B\}} I_{\mu}^k I_{\nu}^k \quad (9)$$

or explicitly as in (10), shown at the top of the page.

- 2) Diffuse the  $g_{\mu\nu}$  coefficients by convolving with a Gaussian of variance  $\rho$ , thereby

$$\tilde{g}_{\mu\nu} = G_{\rho} * g_{\mu\nu} \quad (11)$$

where  $G_{\rho} = \frac{1}{\pi\rho^2} e^{-(x^2+y^2)/\rho^2}$ .

- 3) Change the eigenvalues of  $(\tilde{g}_{\mu\nu})$  such that the largest eigenvalue  $\lambda_1$  is now  $\lambda_1 = -\alpha^{-1}$  and  $\lambda_2 = \alpha$ , for some given positive scalar  $\alpha < 1$ . This yields a new matrix  $\hat{g}_{\mu\nu}$  that is given by

$$(\hat{g}_{\mu\nu}) = \tilde{U} \begin{pmatrix} -\alpha^{-1} & 0 \\ 0 & \alpha \end{pmatrix} \tilde{U}^T = \tilde{U} \Lambda_{\alpha} \tilde{U}^T. \quad (12)$$

A single scalar  $\alpha$  is chosen for simplicity of the presentation. Different eigenvalues can be chosen, like eigenvalues that depend on the original ones. The important idea is to set the original largest eigenvalue to a negative value. This operation inverts the diffusion direction across the color edge and thereby enhance it.

- 4) Evolve the  $k$ th channel via the flow

$$I_t^k = \partial_{\mu} \hat{g}^{\mu\nu} \partial_{\nu} I^k \\ = \text{div} \left( \tilde{U} \begin{pmatrix} -\alpha & 0 \\ 0 & \alpha^{-1} \end{pmatrix} \tilde{U}^T \nabla I^k \right). \quad (13)$$

Inverting the heat equation is an inherently unstable process. However, if we keep smoothing the metric coefficients, and apply the diffusion along the edge (given the positive eigenvalue), we get a coherence-enhancing flow that yields sharper edges and is stable for a short duration of time.

## VI. EXPERIMENTAL RESULTS

We tested the proposed method on four benchmark images that were sampled with Bayer color filter array pattern (see Figs. 4–7). The following examples demonstrate the reconstruction and enhancement results for four benchmark images: statue, sails, window, and lighthouse. For each case, the top left is the original image. As a reference, we present the result of a bilinear interpolation for the missing points for each channel separately at the top right of each figure. The bottom left is the result of the first reconstruction by weighted interpolation step, and the bottom right is the second step enhancement result. To view these images in color, see

[www.cs.technion.ac.il/~ron/demosaic.html](http://www.cs.technion.ac.il/~ron/demosaic.html). The same parameters were used for the reconstruction in all the examples, i.e., case dependent tuning was not used for the different images.

## ACKNOWLEDGMENT

The author is grateful to Prof. J. Sethian for the helpful discussions, and to Dr. Y. Hel-Or for introducing the problem, the helpful discussions that followed, and supplying the color benchmark images.

## REFERENCES

- [1] D. R. Cok, "Reconstruction of CCD images using template matching," in *Proc. IS&T Ann. Conf./ICPS*, 1994, pp. 380–385.
- [2] G. H. Cottet and M. El Ayyadi, "A Volterra type model for image processing," *IEEE Trans. Image Processing*, vol. 7, pp. 292–303, March 1998.
- [3] G. H. Cottet and L. Germain, "Image processing through reaction combined with nonlinear diffusion," *Math. Comput.*, vol. 61, pp. 659–673, 1993.
- [4] P. T. Eliason, L. A. Soderblom, and P. S. Chavez, "Extraction of topographic and spectral albedo information from multi spectral images," *Photogramm. Eng. Remote Sensing*, vol. 48, pp. 1571–1579, 1981.
- [5] B. V. Funt, M. S. Drew, and M. Brockington, "Recovering shading from color images," in *Lecture Notes in Computer Science: Computer Vision, ECCV'92*, vol. 588 G. Sandini, Ed. Berlin, Germany: Springer-Verlag, 1992, pp. 124–132.
- [6] D. Gabor, "Information theory in electron microscopy," *Lab. Investigat.*, vol. 14, pp. 801–807, 1965.
- [7] G. Healey, "Using color for geometry-insensitive segmentation," *J. Opt. Soc. Amer. A*, vol. 6, pp. 920–937, 1989.
- [8] R. Kimmel, R. Malladi, and N. Sochen, "Image processing via the beltrami operator," in *Proc. 3rd Asian Conf. Computer Vision*, Hong Kong, Jan. 1998.
- [9] M. Lindenbaum, M. Fischer, and A. M. Bruckstein, "On Gabor's contribution to image enhancement," *Pattern Recognit.*, vol. 27, pp. 1–8, 1994.
- [10] G. Sapiro and D. L. Ringach, "Anisotropic diffusion of multivalued images with applications to color filtering," *IEEE Trans. Image Processing*, vol. 5, pp. 1582–1586, 1996.
- [11] N. Sochen, R. Kimmel, and R. Malladi, "A general framework for low level vision," *IEEE Trans. Image Processing*, vol. 7, pp. 310–318, 1998.
- [12] J. Weickert, "Anisotropic diffusion in image processing," Ph.D. dissertation, Kaiserslautern Univ., Kaiserslautern, Germany, Nov. 1995.

**Ron Kimmel** was born in Hafia, Israel, in 1963. He received the B.Sc. degree (with honors) in computer engineering in 1986, the M.S. degree in electrical engineering in 1993, and the D.Sc. degree in 1995, all from Technion—Israel Institute of Technology, Haifa.

From 1986 to 1991, he served as an R&D officer in the Israel Air Force. From 1995 to 1998, he was a Post-doctoral Fellow at Lawrence Berkeley National Laboratory, Berkeley, CA, and the Mathematics Department, University of California, Berkeley. He is currently a faculty member of the Computer Science Department, Technion. His research interests are in computational methods and their applications including topics in differential geometry, numerical analysis, nonlinear image processing, geometric methods in computer vision, and numerical geometry methods in computer aided design, robotic navigation, and computer graphics.

Dr. Kimmel was awarded the Alon Fellowship, the HTI Postdoctoral Fellowship, and the Wolf, Gutwirth, Ollendroff, and Jury fellowships during his graduate studies.